PHYSICAL REVIEW C VOLUME 36, NUMBER 2 AUGUST 1987

Structure of unbound states in ^{29}Si from neutron resonance spectroscopy of ^{28}Si + n

H. Weigmann, P. W. Martin,* R. Köhler, I. van Parijs,†
F. Poortmans,‡ and J. A. Wartena
Commission of the European Communities, Joint Research Center, Geel Establishment, Central Bureau for Nuclear Measurements, B-2440 Geel, Belgium
(Received 9 February 1987)

Resonance structure in the ^{28}Si+n system has been investigated by performing neutron total cross section and capture γ-ray measurements. A detailed analysis of resonance parameters was carried out up to a neutron energy of 2.75 MeV. Level densities were determined for s- and p-wave resonances, as well as neutron strength functions and partial radiative widths. The neutron strengths are compared with existing model calculations. The neutron width of at least one $T=\frac{3}{2}$ level has been determined, providing a measure of isobaric spin mixing. Whereas other workers previously reported a strong correlation between the reduced neutron widths (Γ_n^l) and total radiative widths, we observe no significant correlation between Γ_n^l and the partial radiative widths for ground state transitions. We conclude that radiative capture in ^{28}Si+n does not proceed via a simple valence mechanism, but must involve several competing doorway states. The observed $M1$ strength in ^{29}Si is lower than that reported for ^{28}Si from inelastic electron scattering, suggesting either a considerable fragmentation or a significant reduction due to the presence of the additional neutron.

I. INTRODUCTION

Neutron resonances in ^{28}Si + n have been studied by Newson *et al.*[1] in 1977, and apparent doorway structures in their data described by Halderson *et al.*[2] in a core-particle coupling model. The encouraging success of this description suggests the improvement of the experimental data base on ^{28}Si + n resonances; improved resolution should make spin assignments more certain and allow one to extend detailed R-matrix analysis to higher energies, and the inclusion of data on partial radiative widths should help in further understanding the resonance structure.

A $T=\frac{3}{2}$ level is expected to be found as an s-wave resonance at about 1.2 MeV neutron energy which would allow the determination of its isospin impurity, thereby increasing the systematic knowledge on isospin mixing in light nuclei. Cierjacks *et al.*[3] have analyzed data on ^{28}Si + n obtained at Karlsruhe with this aim.

It has been pointed out by several authors[4–7] that because the proton and neutron $d_{5/2}$ subshells in ^{28}Si are closed in an extreme shell model, the ^{28}Si + n system should provide an ideal case for the study of valence effects in the neutron capture process. Indeed, Boldeman *et al.*[4] reported evidence for valence capture by noting a strong positive correlation between the reduced neutron and total radiative widths for p-wave resonances. Partial radiative widths for the two strongest $p_{3/2}$ resonances have been measured by several authors,[5–7] and it was found that the Lane-Mughabghab[8] formulation of the valence model accounts well for the ground state and second excited state transitions, although it fails to explain most of the weaker transitions to other excited states. A quantitative analysis of these ^{28}Si + n resonances was used by Castel and Mahaux[9] to demonstrate that the success of the valence model is due to the dominance of the external contribution to the valence capture integral.

In the higher neutron energy range from 3 to 14 MeV, Lindholm *et al.*[10] found that for transitions to the first and second excited state of ^{29}Si, while a combination of compound nucleus and direct-semidirect processes could account for the nonresonant part of the cross section, the microscopic model of Micklinghoff and Castel[11,12] was required to describe the resonance structure.

Of additional interest is the need to provide data on the magnitude and distribution of the magnetic dipole strength in nuclei. As a sensitive test of shell model calculations, such information may help to elucidate several aspects of the model, including the spin-dependent part of the residual interaction and the role of effective operators. Magnetic dipole strength in even-even s-d shell nuclei has been found to be in accord with open shell model calculations.[13] In particular, since the $d_{5/2}$ subshell is closed in ^{28}Si, one expects the largest $M1$ strength in this nucleus, in agreement with observation.[13,14] This strength is concentrated around 11.5 MeV excitation energy. It is interesting to see whether a corresponding strength can be found also in ^{29}Si, as might be expected in an extreme weak coupling model.

In order to resolve some of these questions, we have undertaken a comprehensive investigation of the ^{28}Si + n system by performing time-of-flight measurements with improved energy resolution for both the total and partial radiative capture cross sections.

II. EXPERIMENTAL DETAILS

The measurements were performed at the neutron time-of-flight spectrometer of the 150 MeV electron linear accelerator of CBNM, Geel. A mercury-cooled uranium target was used to produce a pulsed beam of neutrons

with a repetition rate of 800 Hz and burst widths between 0.7 and 5 ns. Time-of-flight measurement was used to determine the neutron energy with flight paths varying between 130 and 400 m.

A. Total cross section measurements

A standard setup has been used with the transmission sample placed in a sample changer at a distance of 100 m from the neutron source. We used a metallic silicon sample of natural isotopic composition and thickness of 0.07356 atoms/b.

The experiments were carried out with an unmoderated neutron beam, i.e., detecting the neutrons from the uranium target directly. A 2 cm thick uranium filter provided a significant reduction of the γ-flash effect in the detector.

Two series of transmission experiments, both with a 400 m flight path, have been made. In the first run we used as a neutron detector a $15\times15\times2$ cm^3 NE 110 scintillator. Four small photomultipliers, type RCA 4516, were mounted side-on the scintillator, out of the neutron beam. The construction of the detector was such as to keep capture of the incident neutrons by the construction materials very low. In order to optimize the signal-to-background ratio, we divided the pulse-height range into three windows and stored only those time-of-flight events for which the pulse height was within the required window. In this way, the only background component of importance was a nearly constant one due to cosmic radiation and natural radioactivity and to long-lived radiations from the neutron source. This background was determined at long flight times, shortly before the arrival of the next neutron burst. The ratio background-to-signal was minimum in the region of 2 MeV (less than 0.1%), but increased with decreasing neutron flux to a value of 2% at 19 MeV and 10% at 250 keV.

The energy range covered in this run was between 250 keV and 19 MeV. The detector had a timing resolution of 1 ns, the linac burst width was 5 ns, and the time-digitizer channel width was 4 ns.

In the second measurement we used a smaller NE 110 detector with dimensions 5 cm diam$\times$2.5 cm thickness, coupled directly to a RCA 8850 photomultiplier. This detector had a timing resolution of 260 ps. The linac burst width was 700 ps, and the time-digitizer channel width was 312 ps. Data were taken in the energy range from 1.6 up to 6 MeV. The background was less than 0.1% throughout the energy range studied.

B. Capture γ-ray measurements

A neutron flight path of 130 m was used for the capture γ-ray measurements. Direct neutrons from the U target as well as neutrons from two Be-canned water moderators placed below and above the U target were used in these measurements which covered the neutron energy range from 1 keV to 5 MeV. A combination of uranium, lead and B_4C filters was inserted in the neutron beam to reduce the effect of the γ flash and to prevent overlap of low energy neutrons. an ionization chamber containing a thin uranium sample was placed at 30 m from the neutron source to monitor the neutron flux shape by detecting fission fragments from the ^{235}U(n,f) reaction.

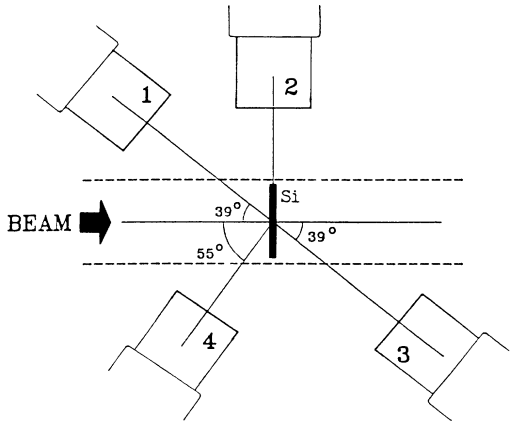

FIG. 1. Experimental layout of the neutron capture γ-ray measurements.

Four 7.5 cm diam and 7.5 cm thick bismuth germanate (BGO) detectors were used in these measurements, mounted as shown in Fig. 1 at angles of 39°, 90°, 125°, and 141° with respect to the neutron beam direction (corresponding to zeros of the Legendre polynomials P_3, P_1, and P_2, respectively). The samples took the form of compressed discs of natural silicon, each 8 cm in diameter, and of thicknesses 8 mm (0.04 atoms/b) and 16 mm (0.07 atoms/b).

The time-of-flight information, together with the γ-ray energy and neutron monitor spectra, were collected in list mode on a Nuclear Data 6600 data acquisition computer. The overall timing resolution of the system was approximately 4 ns.

In order to determine absolute capture yields, some measurements were performed simultaneously with a 2 mm thick iron sample inserted directly in front of the silicon sample, the well-known 1.15 keV resonance in ^{56}Fe (Ref. 15) serving as a reference for normalization of the flux including factors determining the efficiencies and solid angles of the detectors.

III. RESONANCE ANALYSIS

The resonance analysis serves to determine neutron and partial radiative widths as well as spins and parities of the resonances observed in the experimental data.

A. Analysis of the total cross section data

The resonance parameter analysis of the total cross section data has been carried through up to 2.75 MeV neutron energy. Above that energy the resonance structure becomes too complex for a further analysis due to an increased density of observed resonances and growing uncertainty with respect to the inelastic widths.

After correction of the time-of-flight spectra for instrumental dead time and for backgrounds, the neutron energy corresponding to each time-of-flight channel, the total cross section and its statistical error are calculated from

TABLE I. Resonance parameters of ^{28}Si. A denotes J and l obtained from Brookhaven National Laboratory (BNL) Report No. BNL-325 (Ref. 29). B denotes $g\Gamma_n$ obtained from BNL Report No. BNL-325 (Ref. 29). C, D, and E are explained in the text.

E_n (keV)	E_{ex} (keV)	J	l	$g\Gamma_n$ (keV)	$g\Gamma_{n'}$ (keV)	$g\Gamma_n\Gamma_{\gamma f}/\Gamma$ (eV) f=0	f=1273 (keV)	f=2200 (keV)	Remarks
31.74	8504.5	(5/2)	(2)				0.011±0.006		C,D
55.00	8527.0	1/2	0	1.50±0.30					A,B
67.73	8539.3	3/2				0.60±0.06	0.81±0.09	0.30±0.06	C,E
86.97	8557.8						0.05±0.02	0.42±0.05	
188.00	8655.4	1/2	0	60.0±7.0		2.20±0.80			A,B
298.70	8762.2						0.32±0.08	0.22±0.12	
354.10	8815.7	(1/2)	(1)	0.10±0.01			1.64±0.24		
399.50	8859.5	3/2	(2)			0.50±0.06			C,D
532.72	8988.1	5/2	2	1.65±0.06				0.58±0.45	
566.23	9020.4	3/2	1	21.8±1.0		1.71±0.65			
587.20	9040.7	3/2	2	0.55±0.06		0.89±0.11		0.66±0.36	C,E
590.36	9043.7	1/2	0	0.55±0.05					
602.54	9055.5		≥1	0.12±0.02		0.12±0.07		4.2±0.5	
771.63	9218.7		≥1	0.17±0.02			1.05±0.28		
786.20	9232.8	3/2	(2)			0.36±0.16			C,D
804.00	9249.9		(≥2)					2.40±0.40	D
813.38	9259.0	3/2	1	59.4±2.0		3.1±0.9		2.70±1.80	
845.20	9289.7	≥3/2	2	1.06±0.06				0.52±0.40	E
872.25	9315.8		≥1	0.12±0.02				1.07±0.45	
910.13	9352.4	3/2	1	6.80±0.40		0.78±0.22			
966.06	9406.4	1/2	1	81.2±4.0					
974.70	9414.7	3/2	(2)			1.26±0.18			C,D
1017.7	9456.2	≥3/2	≥1	0.24±0.02				1.88±0.46	
1042.8	9480.4	5/2	2	2.70±0.15		0.31±0.15		0.88±0.68	
1085.3	9521.4		(≥2)				0.56±0.33		D
1148.9	9582.8		(≥2)	0.02±0.01			1.04±0.32	1.15±0.36	D
1162.6	9596.1	1/2	0	2.60±0.30		3.5±0.3			
1201.1	9633.2	1/2	0	3.60±0.40					
1201.7	9633.8	1/2	1	18.2±0.5					
1257.0	9687.2	1/2	0	15.6±1.4					
1264.3	9694.2	5/2	2	3.00±0.24		0.74±0.24	1.07±0.60	6.0±1.0	
1380.6	9806.5	3/2	(2)	0.06±0.02		1.19±0.25	1.27±0.53		C,D
1408.7	9833.6	3/2	1	10.6±0.6		2.74±0.64			
1474.6	9897.2		(≥2)				1.42±0.92		D
1479.7	9902.1	3/2	2	7.20±0.40					
1512.2	9933.5		≥1	0.36±0.06					
1528.5	9949.2	3/2	2	5.60±0.40				1.00±0.70	
1580.2	9999.1	≥3/2	≥2	1.80±0.15					
1595.7	10014.1	3/2	1	19.0±1.0			1.16±0.86	1.30±1.02	
1596.5	10014.9		≥2	0.09±0.06					
1639.4	10056.3	5/2	2	51.3±6.0			3.8±2.5	17.9±6.6	
1650.7	10067.2	5/2	2	71.7±6.0					
1658.7	10074.9	1/2	1	1.30±0.30					
1664.9	10080.9		≥2	0.60±0.10					
1785.1	10196.9	≥3/2	≥2	0.50±0.04					
1805.9	10217.0	5/2	2	1.86±0.12					
1848.2	10257.8	5/2	2	67.2±3.0					
1855.6	10265.0		≥2	2.64±1.20			12.3±5.7		
1857.7	10267.0	3/2	1	89.6±8.0		7.4±1.6			
1918.8	10326.0	3/2	1	38.4±4.0	0.50±0.50	10.2±1.5	3.7±2.7		
1928.1	10334.9	≥3/2	≥2	1.23±0.12					
1973.3	10378.6	3/2	2	35.4±4.0	0.52±0.52				
1989.2	10393.9	≥3/2	≥2	0.81±0.06					
2041.6	10444.5	1/2	0	1.80±0.20	0.01±0.01				

TABLE I. (*Continued.*)

E_n (keV)	E_{ex} (keV)	J	l	$g\Gamma_n$ (keV)	$g\Gamma_{n'}$ (keV)	$g\Gamma_n\Gamma_{\gamma f}/\Gamma$ (eV) f=0	f=1273 (keV)	f=2200 (keV)	Remarks
2060.0	10462.2		≥2	2.40±0.60					
2062.4	10464.6	(3/2)	≥1	2.00±0.30	0.02±0.02	2.45±0.63			E
2084.2	10485.6	≥5/2	≥2	1.80±0.15					
2089.7	10490.9	1/2	1	2.10±0.50	0.13±0.13				
2090.5	10491.7	3/2	1	55.2±4.0	3.80±2.00				
2116.7	10517.0	5/2	2	13.8±0.6	3.51±0.45				
2171.0	10569.4		1	7.80±1.00					
2227.6	10624.0	≥3/2	2	15.6±1.0					
2281.4	10675.9		≥2	0.27±0.06					
2282.0	10676.5	3/2	1	48.0±4.0	17.2±2.0				
2373.7	10765.0	≥3/2	2	14.1±0.6					
2445.3	10834.1	1/2	0	10.6±1.0	0.75±0.20				
2459.7	10848.0	(3/2)	2	54.0±6.0	17.0±4.0	2.80±1.30			E
2496.9	10884.0	5/2	2	37.5±1.5	5.70±0.90				
2534.0	10919.8	3/2	1	100.0±20.0	134.0±20.0				
2600.7	10984.1		≥1	2.40±0.60					
2660.7	11042.1	≥5/2	≥2	7.12±0.40					
2695.8	11075.9	1/2	1	5.40±0.40	3.90±0.70				
2730.7	11109.6	1/2	0	2.00±0.30	3.20±0.40				
3134.6	11499.5	3/2				6.9±1.9			C,E
4638.0	12950.6	3/2				25.6±9.2			C,E

the measured spectra. These data are then analyzed with a modified version of the multi-channel multi-level R-matrix code MULTI.[16]

The R-matrix boundary condition $B_l=S_l$ is used in the code. Since the shift function S_l is slightly energy dependent, this boundary condition can be strictly fulfilled only at one energy. However, in the analysis we have assumed $B_l=S_l$ to be valid at all energies which amounts to the use of a slightly energy dependent boundary condition. This has the advantage that the introduction of additional arbitrary parameters is avoided.

Often in R-matrix fits an external R function is introduced in order to account for the influence of unspecified levels outside the energy range analyzed. In the present analysis this was not done, but instead the analysis of any specific energy interval always included the effect of all resonances of Table I. For the same purpose in a survey run the analyzed energy range was extended to 3.3 MeV in order to get rough parameter values of the two broadest resonances (a $3/2^-$ resonance at $E_n=3004$ keV with $g\Gamma_n=38$ keV and $g\Gamma_{n'}=17$ keV and a $1/2^-$ resonance at $E_n=3100$ keV with $g\Gamma_n=22$ keV and $g\Gamma_{n'}\approx 0$) between 2.75 and 3.3 MeV to be included in the resonance data set; the parameters of these two resonances should be regarded as tentative only. Of course, a corresponding procedure can not be followed for bound states possibly influencing the cross section in the lower energy region. This may be the reason why in order to get an optimal fit below 1.1 MeV neutron energy we needed slightly different channel radii (4.5 and 5.0 fm, respectively) for the $1/2^-$ and $3/2^-$ channels rather than the 4.2 fm which were used above that energy as well as at all energies for all other channels.

Examples of fits for four selected energy regions are shown in Figs. 2, 3, 5, and 8. For Figs. 3 and 5, in energy regions where little structure is observed in the cross section, every two or four original channels have been added.

For many resonances the spin and neutron orbital angular momentum can immediately be read from the peak value and the interference pattern of the total cross section. In other cases, however, in particular when several resonances overlap, a number of different spin-parity combinations had to be tried. Above the threshold for inelastic scattering at 1.78 MeV neutron energy, the analysis is complicated by the fact that a resonance can often be equally well fitted assuming two different spin values $(l\pm\frac{1}{2})$ with different inelastic widths.

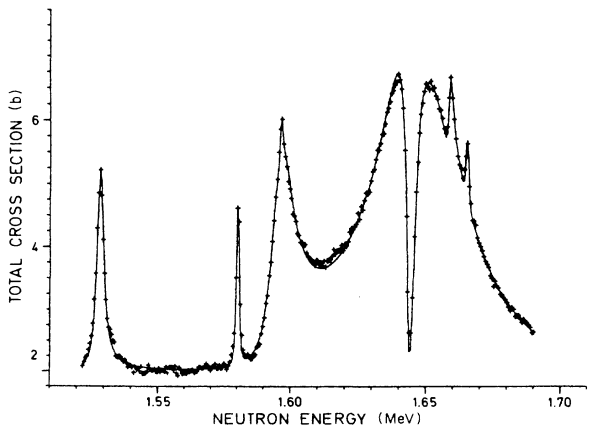

FIG. 2. Example of total cross section data with R-matrix fit, showing the two strong $5/2^+$ resonances at 1.639 and 1.651 MeV neutron energy.

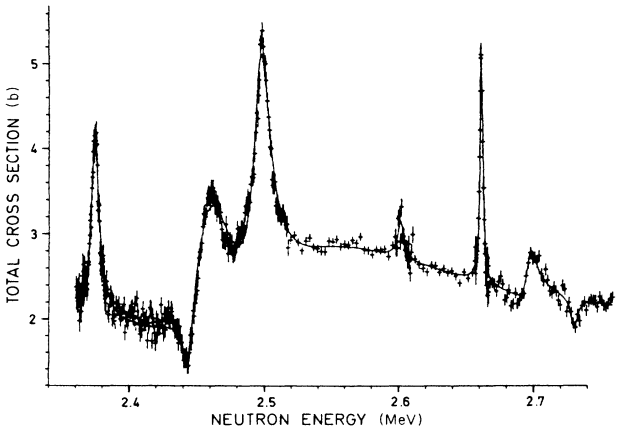

FIG. 3. Example of total cross section data with R-matrix fit between 2.2 and 2.8 MeV neutron energy.

B. Analysis of the radiative capture data

A sample of the radiative capture data, transformed to a linear energy scale, is shown together with the corresponding total cross section in Fig. 4. Three digital windows were set on the γ-ray energy spectra, corresponding to transitions from the resonance to the ground state (0 keV, $1/2^+$), first excited state (1273 keV, $3/2^+$) and the unresolved combination (not shown in Fig. 4) of the second (2028 keV, $5/2^+$) and third (2426 keV, $3/2^+$) excited states of ^{29}Si. An additional window was set at energies above the ground state transition in ^{29}Si. It serves to obtain an estimate of the background due to scattered neutrons which interact in the BGO detectors mainly through the ^{73}Ge(n,γ) reaction.

Using the flux monitor data and the normalization provided by the ^{56}Fe 1.15 keV resonance, capture yields were determined for each resonance within each of the designated pulse height windows. Care was taken to correct the yield in each window for the scattered neutron background and the Compton contribution from higher energy

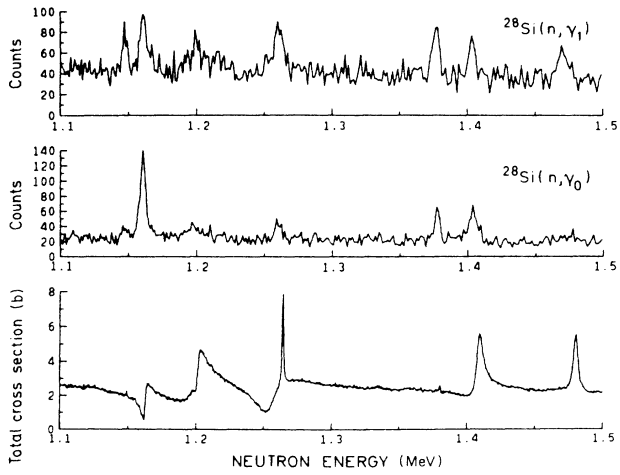

FIG. 4. Example of capture γ-ray data (top two curves) together with total cross section (lower curve).

γ rays. The yield data were then analyzed with the area analysis code TACASI.[17] In this fitting routine, initial guesses are supplied for the resonance neutron (Γ_n) and partial radiative ($\Gamma_{\gamma f}$) widths, and the best fits to the capture areas are obtained by adjustment of any one of these quantities. Corrections for multiple scattering and self-shielding are determined in the course of the fitting procedure.

IV. RESULTS AND DISCUSSION

A. Resonance parameters

In Table I the resonances observed in the present ^{28}Si + n measurements are described. Columns 1 and 2 of the table list the resonance neutron energy E_n (for resonances observed in the total cross section the R-matrix eigen-energy is given) and the excitation energy of the compound nuclear level. In columns 3 and 4 the resonance spin and the neutron orbital angular momentum are indicated. In column 5 the quantity $g\Gamma_n$ as obtained from the analysis of the total cross section is given. For resonances above the threshold for inelastic scattering, column 6 indicates the value of $g\Gamma_{n'}$ used in the total cross section analysis; it is valid only for the resonance spin of column 3. In columns 7 to 9 the quantities $g\Gamma_n\Gamma_{\gamma f}/\Gamma$ obtained from the analysis of the radiative capture data are given. They refer to radiative transitions to the ground state (column 7), the first excited state (column 8) and the unresolved transitions to the second and third excited states (column 9). As long as the total width is given by the neutron width, these quantities are equal to $g\Gamma_{\gamma f}$, and in the following we shall assume that this is true for all resonances of interest in the present study. Errors indicated in columns 7 to 9 include statistical uncertainties, an 8% normalization error, as well as the uncertainty due to the correction for scattered neutrons discussed above. The latter component is particularly large for resonances with large neutron widths. Due to this reason and to the fact that the relatively small γ-ray yield is distributed over a large energy range, we were unable to extract a radiative width for the very broad $1/2^-$ resonance at 966 keV. Finally, the remarks indicated in column 10 refer to the discussion which follows below.

The assignment of resonance spin J and neutron orbital angular momentum l are usually based on the shape of the resonance in the total cross section, i.e., on the peak value of the cross section and on the interference with the potential scattering. Resonances where J and l are assigned on this basis carry no label in column 10. For a number of resonances the spin has been obtained from the angular distribution of the capture γ rays, mostly for $\frac{3}{2}$ to $\frac{1}{2}$ (ground state) transitions. These resonances are labeled C in column 10 of Table I.

Label D refers to the assignment of the orbital angular momentum on the basis of the neutron width, i.e., either the measured $g\Gamma_n$ or its upper limit in cases where no $g\Gamma_n$ value is given in column 5. The upper limit which is the detection limit in the total cross section measurement, is taken to be

$$(g\Gamma_n)_{\text{lim}} = 3\times 10^{-5} E_n \ ,$$

where E_n is the neutron energy of the resonance. The detailed procedure has been the following. From the measured resonances for each J^π value we determine an average reduced neutron width $\langle \Gamma_n^l \rangle$ (see Sec. IV C below). Then, assuming a Porter-Thomas distribution for the reduced neutron widths within each J^π group, the probability is calculated for the occurrence of a neutron width as small or smaller than the one measured for the resonance in question. If the resulting probability is smaller than 5%, we assume the next higher orbital angular momentum for this resonance. Since with this statistical argument the l assignment is in error with a probability of up to 5%, the l value indicated in column 4 of Table I has been put in brackets.

Boldeman *et al.*[4] have made additional l assignments which we have not adopted in Table I, and some of our l values are in disagreement with theirs. Their assignments are based on the ratio of high- to low-bias yield in total capture data, i.e., they test the relative strength of transitions to the ground and first excited states. However, since we may expect a large magnetic dipole strength in ^{29}Si, we do not consider this ratio to be a safe basis for l assignments.

Resonances labeled E in column 10 of Table I deserve a special comment. They are discussed individually below. We first examine the 67.73 keV resonance. This resonance is not covered by our total cross section data, but a rough estimate of its neutron width on the basis of ORNL data[18] yields $g\Gamma_n \approx 5$ eV; with this value the probability for it to be a p wave, calculated as described above, is about 6%. We have thus not indicated any l value for this resonance in Table I. However, we want to point out that there is no good reason for an $l=1$ assignment as proposed in Refs. 4 and 7, but that $l=2$ is indeed much more probable.

Next we look at the 587.20 keV resonance. This resonance is assigned $J=\frac{3}{2}$ from the angular distribution of the ground state transition. The absence of an interference with the broad 566.23 keV resonance in the total cross section then leaves only the choice $J^\pi=3/2^+$.

We now examine the 845.20 keV resonance. The peak total cross section of this resonance indicates that $J \geq \frac{3}{2}$ Again, the absence of an interference with the 813.38 keV resonance then excludes $3/2^-$.

Next we examine the 2062.4 keV resonance. This resonance is part of a hardly resolved doublet (2060.0/2062.4 keV). Regarding the additional uncertainty with respect to the width for inelastic scattering, the total cross section can be reasonably well fitted with four different spin-parity combinations: two of the fits are shown in Fig. 5. Equally acceptable fits are also obtained with the spin-parity combinations $5/2^+ - 3/2^-$ and $3/2^+ - 5/2^+$. However, the latter combination is excluded because of the large ground state radiative width of the 2062.4 keV resonance which would mean an extremely strong $E2$ transition. The other cases will be further discussed in Sec. IV E below.

Now we look at the 2459.7 keV resonance. Only a resonance sequence which includes $l=2$ for this resonance together with a very broad $3/2^-$ state at 2534.0 keV produces an acceptable fit to the total cross section in this energy region (Fig. 3). Due to the uncertainty in the inelastic width, the spin can not be determined from the total cross section. But again the large ground state radiative width suggests $J=\frac{3}{2}$.

Finally, we examine the "resonances" at 3134.6 and 4638.0 keV. As explained above, the detailed resonance analysis has only been performed up to 2750 keV neutron energy. However, the two "resonances" in question have been included in Table I because they represent prominent peaks in the partial capture cross section feeding the ground state of ^{29}Si. These peaks could quite possibly resemble multiplets rather than single resonances. According to the angular distributions of the ground state γ rays, the major components are $J=\frac{3}{2}$ in both cases, and because of the large partial width the 4638 keV level is more probably $J=3/2^-$.

B. Comparison to earlier data

Levels above neutron separation energy have been investigated by charged particle induced transfer reactions,[19–21] including a study of their γ decay by Betz *et al.*[21] A comparison seems to show considerable disagreement for a number of levels. It must be observed, however, that the charged particle data often show only

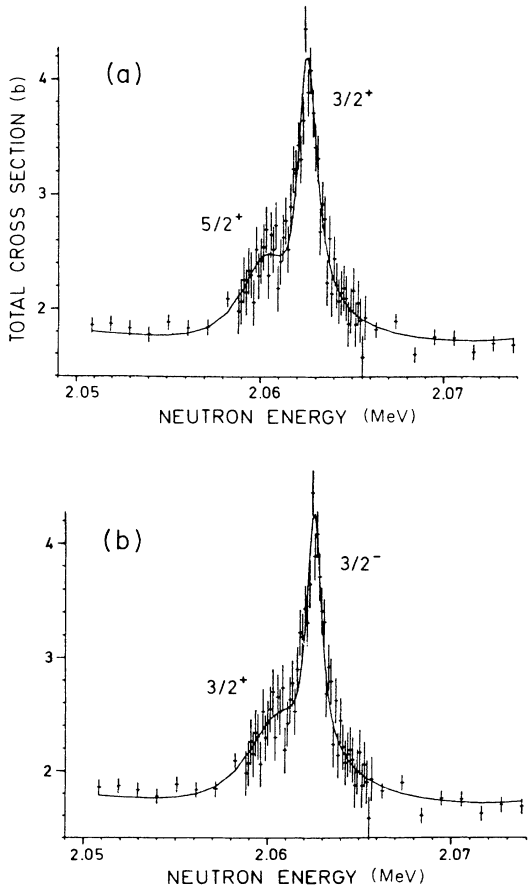

FIG. 5. Two R-matrix fits of the resonance doublet at 2.06 MeV neutron energy with different spin-parity combinations.

one level where we observe several close lying resonances. On the other hand, transfer reactions are more sensitive to higher angular momentum states than are neutron capture measurements, at least at low energies; especially the data of Betz *et al.* preferentially show high angular momentum states. Thus, the apparent discrepancies will often simply result from the observation of different levels.

C. Level density

The spin dependence of the average level spacing is expressed by

$$D(J)=D_0/(2J+1)\exp[-J(J+1)/2\sigma^2] ,$$

where we have taken the spin cutoff parameter σ^2 to be (with $a=0.127A$)

$$\sigma^2=0.146\sqrt{aU}\,A^{2/3}=7.36 .$$

For the determination of the level density from the observed resonances we limit ourselves to s and p waves, because we have to assume that a number of d-wave resonances have been missed. In the case of p-wave resonances we check for missed levels by fitting a Porter-Thomas distribution to the reduced neutron widths. Figure 6 shows as a function of $g\Gamma_n^l$ the number of resonances with a $g\Gamma_n^l$ value larger than the value on the abscissa, together with the fit based on the Porter-Thomas distribution. In Fig. 6(a) only resonances assigned $l=1$ are shown, whereas Fig. 6(b) also includes all resonances for which $l=1$ could not be excluded. In both cases, the larger resonances ($g\Gamma_n^l>10$ eV) are well fitted with essentially the same average spacing, $D(l=1)=145$ keV.

Table II summarizes the results for $l=0,1$. The errors shown are due to the statistical uncertainty of the orthoganal ensemble distribution for a limited sample, and have been determined according to the prescription of Liou and Rainwater.[22]

As a weighted average for D_0 we obtain

$$D_0=(700\pm40)\text{ keV} .$$

It is observed that the values obtained for $l=0$ and $l=1$ agree with that average within the statistical uncertainty.

D. Neutron strength functions

Figure 7 shows the cumulative sums of reduced neutron widths separately for $J^\pi=1/2^+$, $1/2^-$, and $3/2^-$. In addition to the experimental data also the neutron widths of doorway states calculated by Halderson *et al.*[2] are included in the figure. In each of the first two cases, one very strong level is recognized which accounts for more than 80% of the strength observed up to 2.75 MeV neutron energy. For $J^\pi=3/2^-$, several comparatively strong resonances are observed.

Table III summarizes the parameters obtained for these levels, also including the strongest $3/2^+$ and $5/2^+$ resonances. Besides $g\Gamma_n$, the table gives the reduces widths

$$\gamma_n^2=\Gamma_n/2kR\nu_l$$

also shown in Figs. 7, and the ratios γ_n^2/γ_W^2, where the

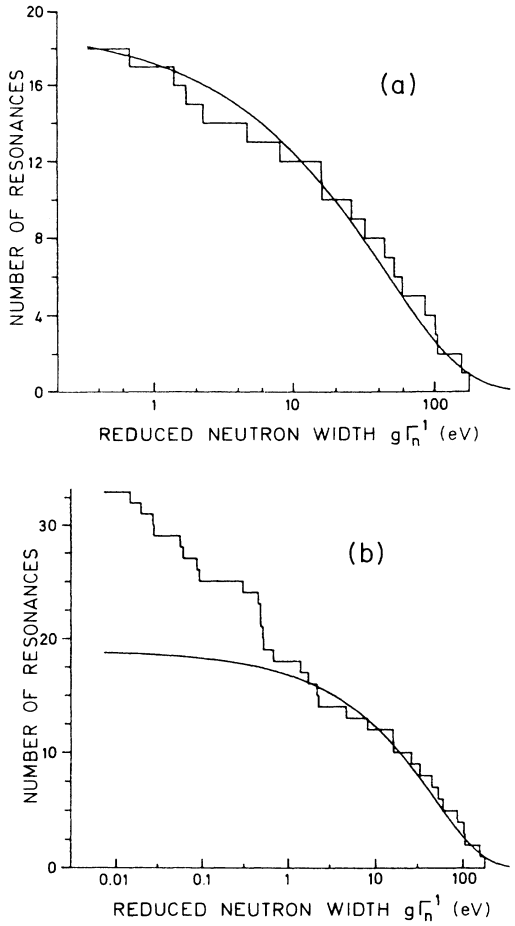

FIG. 6. Integral distributions of reduced neutron widths for p-wave resonances and fits with Porter-Thomas distributions: (a) including identified $l=1$ resonances only; the fit curve is for $D(l=1)=143$ keV; (b) including all resonances for which $l=1$ could not be excluded; the fit curve is for $D(l=1)=147$ keV.

Wigner limit is calculated as

$$\gamma_W^2=\frac{\hbar^2}{mR^2}=2.1\text{ MeV} .$$

$R=4.5$ fm is used to calculate γ_n^2 and γ_W^2.

It is seen that the strong resonances present in Fig. 7 as well as the three strong $5/2^+$ levels represent indeed considerable fractions of the Wigner limit and thus will reflect fairly simple configurations.

The $1/2^+$ doorway state is proposed by Halderson *et al.* to be a 2p-1h state (with respect to a ^{28}Si core) of configuration $(f_{7/2})^2(d_{5/2})^{-1}$. It is hardly conceivable

TABLE II. Observed average level spacings.

l	$D(l)$ (keV)	D_0 (keV)
0	332^{+39}_{-32}	631^{+74}_{-62}
1	145±9	725±45

that this configuration could contribute to the relatively large ground state γ ray width observed for the 188 keV resonance. In fact, the $M1$ strength is expected to be mainly connected to spin-flip transitions, i.e., to states with either a neutron or a proton $(d_{3/2})$-$(d_{5/2})^{-1}$ particle hole pair plus an $s_{1/2}$ neutron. We thus assume that a sizeable fraction of such configurations is admixed in the 188 keV resonance. It is interesting to note that the other $1/2^+$ resonance carrying a large ground state γ-ray strength has only a very small neutron width.

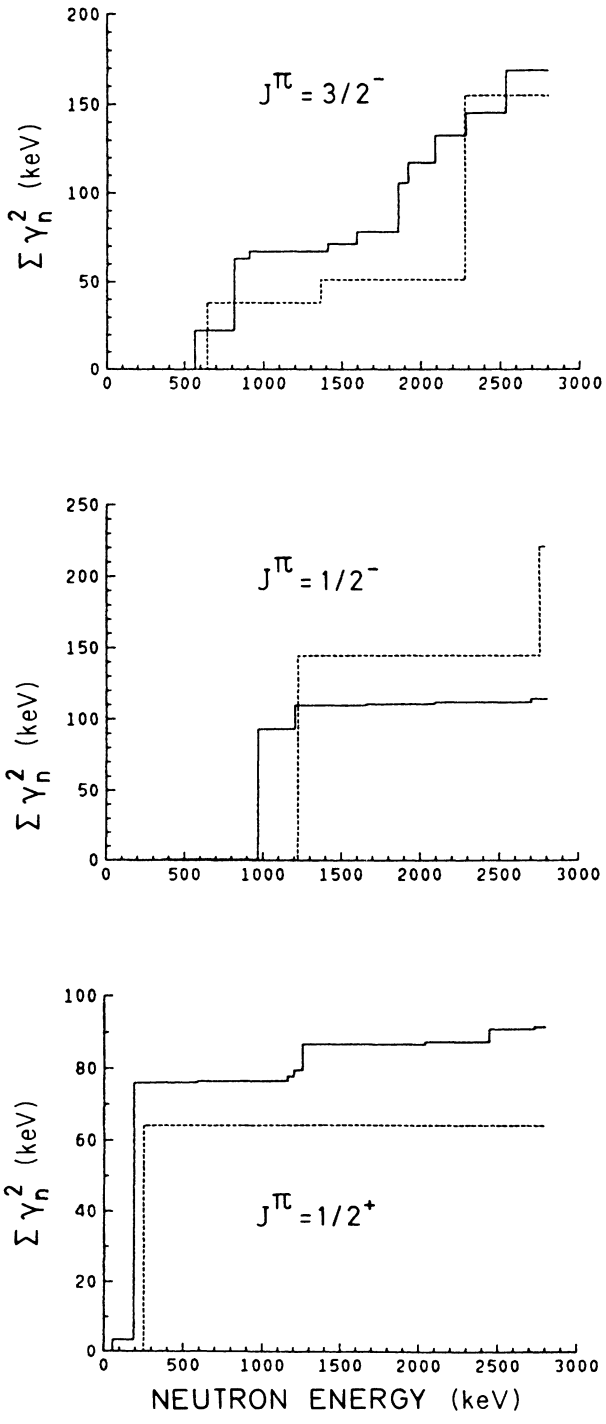

FIG. 7. Cumulative sums of reduced neutron widths γ_n^2 for $J^\pi = 1/2^+$, $1/2^-$, and $3/2^-$ resonances. Solid lines, present experimental data; dashed lines, model calculations of Halderson *et al.* (Ref. 2).

In the case of $1/2^-$ resonances, the doorway state calculations of Halderson *et al.* reproduce fairly well the strong resonance at 966 keV neutron energy. However, we do not observe the second strong state predicted at 2.75 MeV (and seen by Newson *et al.*[1] at about 2.6 MeV). Also in the higher neutron energy range not analyzed in detail, the measured cross section does not show evidence for such a state.

Halderson *et al.* predict a $3/2^-$ doorway state at 640 keV neutron energy with main wave function components $[p_{3/2}\times 0^+]$ and $[d_{3/2}\times 3^-]$ which should correspond to the two strong resonances observed at 566 and 813 keV, although the calculated strength is only about 60% of the experimental one. Additional strength is found experimentally at 1.9 MeV and again around 2.5 MeV. It might correspond to the very strong doorway state predicted by Halderson *et al.* at 2.27 MeV. It is interesting to note that the resonances observed at 2.282 and 2.534 MeV show a very large strength in the inelastic channel to the 2^+ first excited state of ^{28}Si, corresponding to reduced widths of 24 and 109 keV, respectively. A candidate for this strength might be the configuration $[p_{3/2}\times 2^+]$ which according to Halderson *et al.* also contributes mainly to the strong $1/2^-$ doorway at 966 keV.

Finally, Table IV lists the overall neutron strength functions

$$S(J;l)=\frac{\Sigma\Gamma_n^l}{E_{\max}};\quad \Gamma_n^l=\Gamma_n/v_l(1\text{ eV}/E_n)^{1/2}\ ;$$

$$E_{\max}=2.75\text{ MeV}\ ,$$

as obtained from the parameters of the definitely assigned resonances. The correction factor of Liou and Rainwater[22] to be applied for a limited sample of Porter-Thomas distributed widths has been included, and again the error has been calculated according to the prescription of Ref. 22.

TABLE III. Parameters of the strongest resonances.

E_n (keV)	J^π	$g\Gamma_n$ (keV)	γ_n^2 (keV)	γ_n^2/γ_W^2 (%)
188.0	$1/2^+$	60	72.5	3.44
966.1	$1/2^-$	81.2	92.5	4.38
566.23	$3/2^-$	21.78	22.3	1.06
813.38	$3/2^-$	59.4	40.6	1.92
1857.7	$3/2^-$	89.6	27.4	1.30
2534.0	$3/2^-$	100.0	23.6	1.12
1973.3	$3/2^+$	35.4	36.0	1.71
2459.7	$3/2^+$	54.0	37.3	1.77
1639.4	$5/2^+$	51.3	49.3	2.34
1650.7	$5/2^+$	71.7	68.0	3.22
1848.2	$5/2^+$	67.2	51.5	2.44

TABLE IV. Neutron strength functions.

J^π	$S(J,l)$ (10^{-4})
$1/2^+$	$0.69^{+0.49}_{-0.25}$
$1/2^-$	$0.88^{+0.84}_{-0.38}$
$3/2^-$	$1.25^{+0.82}_{-0.44}$
$3/2^+$	$0.77^{+0.54}_{-0.28}$
$5/2^+$	$1.68^{+1.10}_{-0.59}$

E. Isobaric analogue states

Figure 8(a) shows the fit to the measured total cross section in the region of the expected $(J^\pi;T)=(1/2^+;3/2)$ level, the isobaric analog to the first excited state in ^{29}Al. We identify the resonance at 1201 keV as the $T=\frac{3}{2}$ level which yields an excitation energy of $E_{ex}(T=\frac{3}{2})=9633.6$ keV, in excellent agreement with the ^{30}Si(^{3}He,α)^{29}Si measurement of Detraz and Richter.[23] This is in contrast to an earlier analysis of ^{28}Si neutron cross sections by Cierjacks *et al.*[3] who did not observe the 1201 keV s-wave resonance and identified the 1163 keV resonance with the expected $T=\frac{3}{2}$ level. The cross section calculated from the resonance parameters of Cierjacks *et al.* is compared to the present experimental data in Fig. 8(b).

Using the equations given, e.g., in Ref. 24 and the parameters of s-wave resonances of Table I, we calculate a "zero order" estimate M_0 and a lower limit $M_{\min}$ of the average isospin mixing matrix element as

$$M_0=\langle T=\tfrac{3}{2}\mid V\mid i\rangle_0=22.2\ \text{KeV}\ ,$$

$$M_{\min}=\langle T=\tfrac{3}{2}\mid V\mid i\rangle_{\min}=14.1\ \text{keV}\ .$$

These two figures are not very different because a single $T=\frac{1}{2}$ level, namely the one at 1257 keV neutron energy, predominates the isospin admixture in the $T=\frac{3}{2}$ level. On the other hand a mixing matrix element of 22 keV is sufficiently large compared to the energy difference between the 1257 keV and the 1201 keV $(T=\frac{3}{2})$ levels that first order perturbation may no longer be justified. Therefore, we have also dealt with the mixing between these two levels in an "exact" two-level treatment: Using again the formulas given in Ref. 24 (Eq. 6 of that reference), we arrive at a mixing matrix element of

$$M=\langle T=\tfrac{3}{2}\mid V\mid T=\tfrac{1}{2}(1257\ \text{keV})\rangle=21.2\ \text{keV}$$

thus very close to the above "zero order" estimate. The observed value compares reasonably well with those of neighboring nuclei (see, e.g., Ref. 25).

The isobaric analogue to the $3/2^+$ third excited state of ^{29}Al may be expected between 2.0 and 2.1 MeV neutron energy. Possible candidates are the two close-lying resonances at 2060.0 and 2062.4 keV shown in Fig. 5. To fit the 2060.0 keV resonance as $3/2^+$ [Fig. 5(b)] requires a large inelastic neutron width of 3.1 keV which is very improbable for a $T=\frac{3}{2}$ level. However, the spin-parity combination of Fig. 5(a) leads to parameters for the 2062.4 keV $3/2^+$ resonance consistent with a $T=\frac{3}{2}$ assignment: using the parameters of $3/2^+$ resonances of Table I, a perturbation treatment like the one mentioned above yields for the average isospin mixing matrix element a "zero order" estimate M_0 and a lower limit $M_{\min}$ of

$$M_0=19\ \text{keV};\quad M_{\min}=13\ \text{keV}\ .$$

We have not been able to identify the isobaric analogue to the $3/2^+$ fourth excited state of ^{29}Al, although this state has been observed in the ^{30}Si(^{3}He,α) work of Detraz an Richter,[23] and thus its energy is known to correspond to 2710 keV neutron energy. The 2695.8 keV resonance is excluded as a candidate for two reasons. The fit of that resonance with a $3/2^+$ assignment is worse than the one for the $1/2^-$ assignment shown in Fig. 3, and again a $3/2^+$ assignment would require an overly large inelastic

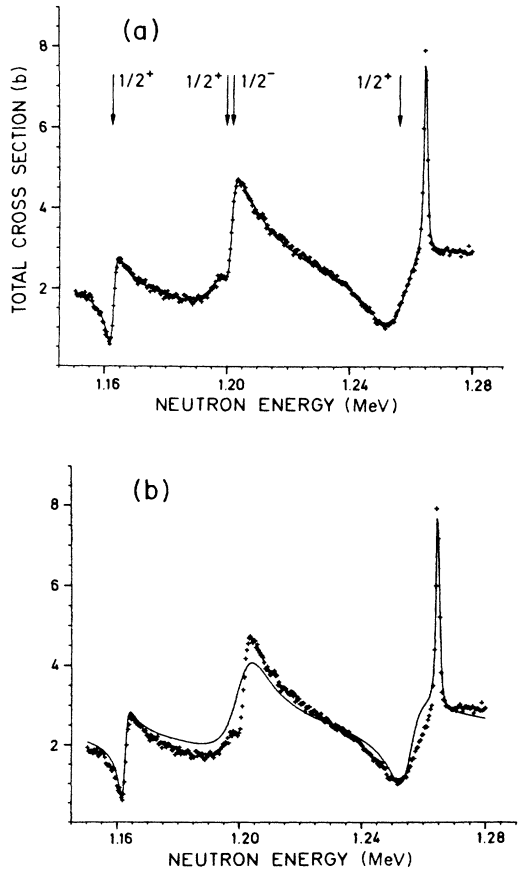

FIG. 8. R-matrix fit of total cross section data around the lowest $T=\frac{3}{2}$ level with $J^\pi=\frac{1}{2}$: (a) fit with present resonance parameters; (b) curve calculated with parameters of Ref. 3 .

neutron width. We have thus to conclude that the neutron width of the state seen by Detraz and Richter is below the detection limit of the present experiment. The fact that the ^{30}Si(^{3}He,α) reaction strongly populates a $T=\frac{3}{2}$ state not populated in ^{28}Si + n, and vice versa for the possible isobaric analogue of the third excited state of ^{29}Al discussed above, should not be looked at as a contradiction, but rather as suggestive with respect to the nuclear structure of these states.

F. Radiative strengths

Tables V–VII summarize measured partial radiative widths $g\Gamma_{\gamma 0}$ for ground state transitions from resonances with $J=3/2^-$, $1/2^+$, $3/2^+$, and the corresponding reduced transition strengths. In Table V electric dipole transitions from $3/2^-$ resonances are shown. It includes the two high energy "resonances" at 3.1 and 4.6 MeV neutron energy. The sum of measured reduced transition probabilities is 4.03×10^{-2} e^{2}fm^2. However, the strengths of the 3.1 and 4.6 MeV states could actually be larger than indicated in the table: the widths of these resonances for inelastic neutron emission may be significant and hence the measured quantities $g\Gamma_n\Gamma_{\gamma 0}/\Gamma$ smaller than $g\Gamma_{\gamma 0}$.

A correlation analysis of the $3/2^-$ resonances below 2.75 MeV neutron energy was performed in order to check for the influence of valence transitions. Apart from those of Table V, four additional $3/2^-$ resonances (at 1596, 2090, 2282, and 2534 keV) were considered. Since no ground state transitions had been observed for these resonances, a transition strength of half the detection limit, which is estimated as

$$B(E1)_{\rm lim}=\exp[1.1E_n\ ({\rm MeV})-9.4]{\rm e}^2{\rm fm}^2\ ,$$

was used in the correlation analysis. The calculated correlation coefficient was

$$\rho[\gamma_n^2,B(E1)]=0.25\ (0.30)\ ,$$

where the value in brackets arises when we limit ourselves to the seven resonances below 2 MeV (if the 2062.4 keV resonance is assigned $3/2^-$ and is included in the complete set, no change occurs). The probabilities for accidental occurrence of these correlation coefficients on the basis of Porter-Thomas fluctuations of the partial widths, are $P=0.23$ and 0.24, respectively. Thus, there is no clear evidence for a simple valence mechanism in the $3/2^-$ resonance capture. This is in contrast to the results obtained by Boldeman *et al.*[4] and Jackson and Toohey.[26] However, Boldeman *et al.* have treated all p-wave resonances together, and the extremely strong $1/2^-$ resonance at 966 keV neutron energy contributed significantly to the overall correlation. For the reasons mentioned in Sec. IV A we were unable to extract a radiation width for this resonance. Furthermore, in both, the work of Boldeman *et al.* and Jackson and Toohey, a number of resonances were included in the correlation analysis which according to our analysis are probably d wave. It is obvious that the inclusion of d-wave resonances will produce spurious correlations because both neutron widths and radiative widths which then are $M1$ or (in the case of $5/2^+$ resonances) $E2$ in character, will tend to be small.

The fact that we do not observe a strong correlation indicates that the capture mechanism in ^{29}Si is more complex than envisaged by the simple valence model. For example, a suppression of $[\gamma_n^2,B(E1)]$ correlations would arise if besides the $[p_{3/2}\times0^+]$ state other simple configurations like the $[d_{3/2}\times3^-]$ suggested by Halderson *et al.*, would contribute significantly to the neutron or radiative widths. Indeed, recently Kitazawa *et al.*[27] succeeded in reproducing the partial radiative widths of the 566 keV $3/2^-$ resonance in a particle-vibration coupling model which includes besides the $[d_{3/2}\times3^-]$ also the $[f_{7/2}\times2^+]$ doorway configurations.

It is interesting to note that two dominant peaks at 9.2 and 10.3 MeV excitation energy were observed by Pywell *et al.*[28] in the ^{29}Si(γ,n) cross section. According to our data, the $3/2^-$ resonances which we resolve at 566 and 813 keV neutron energy are the main components of the former peak, whereas the latter one will mainly be due to the resonances at 1858 and 1919 keV, also with spin $3/2^-$.

A strong fairly isolated peak in the ^{28}Si(n,γ_0) cross section at 4.6 MeV neutron energy was also observed by Lindholm *et al.*[10] Our resonance at 4.638 MeV (the last entry in Table I) agrees with their spin assignment of $J=\frac{3}{2}$, but our partial width is only about 64% of their estimate.

Tables VI and VII give details for the magnetic dipole

TABLE V. Electric dipole transitions from $3/2^-$ resonances.

E_n (keV)	$g\Gamma_{\gamma 0}$ (eV)	$B(E1)$ (e^{2}fm^2)
566.23	1.71	0.22×10^{-2}
813.38	3.11	0.37×10^{-2}
910.13	0.78	0.09×10^{-2}
1408.7	2.74	0.27×10^{-2}
1857.7	7.4	0.65×10^{-2}
1918.8	10.2	0.88×10^{-2}
3134.6	6.9	0.43×10^{-2}
4638.0	25.6	1.12×10^{-2}

TABLE VI. Magnetic dipole transitions from $1/2^+$ resonances.

E_n (keV)	$g\Gamma_{\gamma 0}$ (eV)	$B(M1)\uparrow(\mu_0^2)$
188.0	2.2	0.293
1162.6	3.5	0.342

TABLE VII. Magnetic dipole transitions from $3/2^+$ resonances.

E_n (keV)	$g\Gamma_{\gamma 0}$ (eV)	$B(M1)\uparrow(\mu_0^2)$
67.73	0.60	0.083
399.5	0.50	0.062
587.2	0.89	0.104
786.2	0.36	0.039
974.7	1.26	0.130
1380.6	1.19	0.109
(2062.4)	(2.45)	(0.185)
2459.7	3.70	0.250

transitions from $1/2^+$ and $3/2^+$ resonances. With respect to Table VI, it is interesting to note that comparatively strong ground state transitions are observed for two of the $1/2^+$ resonances, but none for the others, including the $T=\frac{3}{2}$ level at 1201.1 eV neutron energy. The latter case may be understood in the following way, again based on a ^{28}Si core: As mentioned earlier, the $M1$ strength is expected to be mainly connected to spin-flip transitions, i.e., to configurations of the type $(d_{3/2})(d_{5/2})^{-1}(vs_{1/2})$. In contrast, the analogue to the $1/2^+$ first excited state of ^{29}Al would mainly consist of configurations

$$(\pi s_{1/2})^2(\pi d_{5/2})^{-2}(vs_{1/2})$$

or

$$(\pi s_{1/2})(\pi d_{5/2})^{-1}(vs_{1/2})^2(vd_{5/2})^{-1} ,$$

which with respect to the ^{29}Si ground state are $2p$-$2h$ excitations.

In Table VII the resonance at 67.7 keV neutron energy has been included because the parity is more likely to be positive as discussed in Sec. IV A; on the other hand, the resonance at 2062.4 keV is put in brackets owing to the uncertainty of the parity assignment.

The total $M1$ strength detected is $0.64\mu_0^2$ for the $1/2^+$ resonances plus $0.78\mu_0^2$ or $0.96\mu_0^2$ for the $3/2^+$ resonances without or with the doubtful 2062.4 keV level. This is in contrast to the value of $B(M1)\uparrow=5.9\mu_0^2$ reported by Berg *et al.*[13] and Schneider *et al.*[14] for ^{28}Si. However, most of the strength found by these authors is concentrated in a state at 11.445 MeV excitation energy. It is not excluded from our analysis that the strongly radiating resonance at 3134.6 keV ($E_{ex}=11.499$ MeV) is $3/2^+$, too. If so, and if its measured strength is not reduced by a sizeable inelastic scattering contribution, it would contribute another $0.39\mu_0^2$ to the total $B(M1)\uparrow$ in ^{29}Si. Additional $M1$ strength may be hidden in a number of weak levels in the excitation energy region from 11 to 13 MeV, where our detection sensitivity is decreasing. We estimate this missed strength to be less than about $0.2\mu_0^2$ per level. Thus, if the total $M1$ strength in ^{29}Si were comparable to that in ^{28}Si, a considerable fragmentation (into roughly 20 levels) would be implied. It is also conceivable, however, that the additional neutron in ^{29}Si could occupy a $d_{3/2}$ state with a non-negligible probability, thus blocking spin-flip transitions into this state. Indeed, a sizeable $[d_{3/2}\times 2^+]$ admixture in the ^{29}Si ground state was assumed by Kitazawa *et al.*[27] in their particle-vibration calculation.

V. CONCLUSION

The unbound states in ^{29}Si studied in the present work provide a number of interesting features: doorway type structures are seen in several neutron channels, including the ^{29}Si$(5/2^+)\rightarrow{}^{28}$Si(g.s.)$+$n and the ^{29}Si$(3/2^-)\rightarrow{}^{28}Si(2^+)+$n channels. The measured neutron widths of one and a possible second $T=\frac{3}{2}$ isobaric analog states allow the investigation of isospin mixing. The detected $M1$ strength is considerably weaker than in ^{28}Si, suggesting either strong fragmentation or a true reduction. It would be interesting to see to what degree these features can be reproduced by extended nuclear structure calculations.

We wish to thank L. Mewissen for his skillful help in part of the measurements. Thanks are due to J. M. Salomé and the CBNM linac operation team for their continuous effort.

*Permanent address: Physics Department, University of British Columbia, Vancouver, V6T 2A6, Canada.
†Also at Studiecentrum voor Kernenergie/Centre d'Etude de l'Energie Nucléaire, Mol, Belgium.
‡Present address: Laboratorium voor Fysiologie, Vrije Universiteit Brussel, 1090 Brussel, Belgium.

[1]H. W. Newson, W. F. E. Pineo, B.-H. Choi, J. M. Clement, and M. Divadeenam, Ann. Phys. (N.Y.) **103**, 121 (1977).
[2]D. Halderson, B. Castel, M. Divadeenam, and H. W. Newson, Ann. Phys. (N.Y.) **103**, 133 (1977).
[3]S. Cierjacks, S. K. Gupta, and I. Schouky, Phys. Rev. C **17**, 12 (1978).
[4]J. W. Boldeman, B. J. Allen, A. R. de L. Musgrove, and R. L. Macklin, Nucl. Phys. **A252**, 62 (1975).
[5]M. Shimizu, M. Igashira, K. Terazu, and H. Kitazawa, Nucl. Phys. **A452**, 205 (1986).
[6]S. Joly, G. Grenier, J. Voigner, and J. W. Boldeman, Nucl. Phys. **A334**, 269 (1980).
[7]M. J. Kenny, B. J. Allen, J. W. Boldeman, and A. M. R. Joye, Nucl, Phys. **A170**, 164 (1976).
[8]A. M. Lane and S. F. Mughabghab, Phys. Rev. C **10**, 412 (1974).
[9]B. Castel and C. Mahaux, Z. Phys. A **318**, 31 (1984).
[10]A. Lindholm, L. Nilsson, I. Bergquist, R. Zorro, N. Olsson, B. Castel, and A. Likar, Z. Phys. A **317**, 149 (1984).
[11]M. Micklinghoff and B. Castel, Z. Phys. A **282**, 117 (1977).
[12]M. Micklinghoff and B. Castel, Ann. Phys. (N.Y.) **114**, 452 (1978).
[13]U. E. P. Berg, K. Ackermann, K. Bangert, C. Bläsing, W. Naatz, R. Stock, K. Wienhard, M. K. Brussel, T. E. Chapuran, and B. H. Wildenthal Phys. Lett. **140B**, 191 (1984).
[14]R. Schneider, A. Richter, A. Schwierczinski, E. Spamer, O. Titze, and W. Knüpfer, Nucl. Phys. **A323**, 13 (1979).
[15]R. E. Chrien, M. R. Bhat, and O. A. Wasson, Phys. Rev. C **1**, 973 (1970); and R. E. Chrien, private communication.
[16]G. F. Auchampaugh, Los Alamos National Laboratory Scientific Report No. LA-5473-MS, 1974 (unpublished).
[17]F. H. Frohner, General Atomic, Report No. GA-6906, 1966.
[18]D. C. Larson, C. H. Johnson, J. A. Harvey, and N. W. Hill, Oak Ridge National Laboratory Report No. ORNL-TM-5618, 1976.
[19]L. R. Medsker, H. E. Jackson, and J. L. Yntema, Phys. Rev. C **9**, 1851 (1974).
[20]R. J. Peterson, C. A. Fields, R. S. Raymond, J. R. Thieke, and J. L. Ullman, Nucl. Phys. **A408**, 221 (1983).

[21]P. Betz, E. Bitterwolf, A. Burkard, F. Glatz, F. Heidinger, Th. Kern, R. Lehmann, S. Norbert, H. Ropke, C. Schneider, and J. Siefert, Z. Phys. A **309**, 163 (1982).
[22]H. I. Liou and J. Rainwater, Phys. Rev. C **6**, 435 (1972).
[23]C. Detraz and R. Richter, Nucl. Phys. **A158**, 393 (1970).
[24]C. R. Jungmann, H. Weigmann, L. Mewissen, F. Poortmans, E. Cornelis, and J. P. Theobald; Nucl. Phys. **A386**, 287 (1982).
[25]H. Weigmann, Proceedings of the International Conference on Nuclear Data for Basic and Applied Science, Santa Fe, New Mexico, 1985 (unpublished); Radiat. Eff. **94**, 179 (1986).
[26]H. E. Jackson and R. E. Toohey, Phys. Rev. Lett. **29**, 379 (1972).
[27]H. Kitazawa, M. Ohgo, T. Uchiyama, and M. Igashira, Nucl. Phys. **A464**, 61 (1987).
[28]R. E. Pywell, B. L. Berman, P. Kean, and M. N. Thompson, Nucl. Phys. **A369**, 141 (1981).
[29]S. F. Mughabghab, M. Divadeenam, and N. E. Holden, *Neutron Cross Sections* (Academic, New York, 1981), Vol. 1, Part A, where $Z=1-60$.